Geophysical Research Letters

Supporting Information for

Basement topography and sediment thickness beneath Antarctica's Ross Ice Shelf

M.D. Tankersley[1,2], H.J. Horgan[1], C.S. Siddoway[3], F. Caratori Tontini[2,4], K.J. Tinto[5]

[1]Antarctic Research Centre, Victoria University of Wellington, Wellington, New Zealand
[2]GNS Science, Lower Hutt, New Zealand
[3]Colorado College, Colorado Springs, CO, USA
[4]University of Genova, Genova, Italy
[5]Lamont-Doherty Earth Observatory, Columbia University, Palisades, NY, USA

Contents of this file

Text S1 to S7
Table S1
Figures S1 to S6

Introduction

This supplement provides additional information on the assumptions behind the process of determining basement depth from magnetic anomalies (**Text S1),** the collection and processing of aeromagnetic line data (**Text S2**), the methodology of tying ROSETTA-Ice magnetic basement to ANTOSTRAT acoustic basement (Brancolini et al., 1995), through the use of Operation IceBridge (OIB) magnetic data (Cochran et al. 2014) (**Text S3 and S4**), the gridding, merging, and filtering of the resulting basement grid (**Text S5**), the calculation of sediment thickness and β-factors for the region (**Text S6**), and our quantification of uncertainties and comparison with points of previously measured sediment thickness (**Text S7**). Sediment thickness comparisons with past seismic surveys are included in **Table S1**. Also included are supplementary figures showing various additional Ross Ice Shelf grids (**Figure S1**), the Werner deconvolution solutions of OIB flight 403.3 (**Figure S2**), several selected ROSETTA-Ice flight lines with Werner deconvolution solutions (**Figure S3**), unfiltered basement solutions with flight line locations and individual Werner deconvolution solutions (**Figure S4**), uncertainties applied to basement and sediment thickness results (**Figure S5**), and misfit distributions between OIB, ANTOSTRAT, and ROSETTA basement models (**Figure S6**). Python code, within a Jupyter notebook, documents our workflow and figure creation and is accessible here: https://zenodo.org/badge/latestdoi/470814953 or at the GitHub repository: https://github.com/mdtanker/RIS_basement_sediment. Results in the form of netCDF's and csv's are available at https://doi.pangaea.de/10.1594/PANGAEA.941238, including figures of all ROSETTA-ice flight line basement solutions.

Text S1. Depth to basement assumptions

Our resulting basement grid is the depth to the shallowest magnetic signal. It is assumed that the crystalline basement in this region produces significantly larger magnetic anomalies compared to the overlying sediment fill. Note that in some instances, such as igneous bodies intruded into sedimentary basin fill, Werner-determined solutions fall upon the crest of the intrusion, and the actual top of the crystalline basement could be at a deeper level. Intrusions of small lateral extent will have small widths, resulting in small values of parameter S (susceptibility x width) and therefore will be removed by our filter (Text S3). For larger intrusions into existing basins, (i.e. Ross Island and Minna Bluff (Cox et al., 2019)), the modeled magnetic basement surface will be shallower than the bottom of the sedimentary basin. While this underestimates sediment volume, it better characterizes the competency of the substrate from an ice dynamics perspective. This is similar to how extensive intrusions into basins would be imaged by seismic surveys as shallow basement. However, these extensive regions of late-Cretaceous-Cenozoic magmatism are not expected to be prevalent under the RIS (Andrews and LeMasurier, 2021).

Text S2. Magnetic data collection, processing, and Werner deconvolution

Both ROSETTA-Ice and OIB data sets were collected with a Scintrex CS3 Cesium magnetometer. Average flight speeds were 123 m/s and 93 m/s for OIB and ROSETTA-Ice respectively. Altitudes for the sections of OIB flight 403 used here average around 400 m above sea level, while ROSETTA-Ice altitude averaged at 750 m above the ice sheet surface. OIB data were resampled from 20Hz to 1Hz to match the frequency of the ROSETTA-Ice data. Both datasets have been despiked, diurnally corrected, and had the International Geomagnetic Reference Field model removed. See Tinto et al. (2019) for more details of the ROSETTA-Ice survey and flight line locations. Due to variable flight elevations, both between and within the datasets, all magnetic data were upward-continued to 1000 m above sea level. To avoid artifacts of downwards continuing, any data with flight elevations above 1000 m were removed (~10% of the data).

Here we use 2D Werner deconvolution (Werner, 1953), applied to aeromagnetic line data, to image the shallowest magnetic signals in the crust. Assuming that the overlying sediments produce smaller magnetic anomalies than the crystalline basement, we treat the resulting solutions as a depth to the magnetic basement. During Werner deconvolution, moving and expanding windows are passed over the magnetic anomaly line data. Within each window, after linearly detrending the data, the source parameters of the anomalies are estimated with a least-squares approach, assuming the source bodies are infinite-depth dikes or contacts. The source parameters include position (distance along profile and depth), magnetic susceptibility, and source geometry (contact or dike). Solutions are considered valid between 1200 m and 20 km of upward continued flight elevation (approx. 200 m - 19 km bsl). Windows ranged from 500 m - 50 km, with a window shift increment of 1 km and an expansion of 1 km.

Due to passing over the data many times with varying window widths, Werner deconvolution produces a depth-scatter of solutions, which tend to cluster vertically beneath the true magnetic sources. Each of these solutions consists of location, depth, susceptibility (S), window width (W), and a simplified source geometry (dike or contact). For contact-type solutions, parameter S is the estimated magnetic susceptibility of the

body, while for dike-type solutions, S is the product of susceptibility and dike width. During filtering (Text S3-4), a cut-off based on parameter S is used to remove shallow solutions. Since the value of parameter S for contact solutions are typically much smaller than for dike solutions (since they are not multiplied by dike width), only dike solutions have been considered here. To achieve a basement surface from this resulting depth-scatter of solutions, we have utilized parameter-based filtering and clustering, described in Text S3-4. This Werner deconvolution process was the same for both OIB and ROSETTA-Ice magnetics data. Werner deconvolution was performed in Geosoft's *Oasis Montaj* and subsequent processing of these results was performed in Python, and is included in a Jupyter notebook; https://zenodo.org/badge/latestdoi/470814953.

This magnetic basement approach has been used to map sedimentary basins throughout Antarctica, including the Ross Sea (Karner et al., 2005), western Marie Byrd Land (Bell et al., 2006), and Wilkes Subglacial Basin (Studinger et al., 2004; Frederick et al., 2016). Our approach is similar to past studies, but our proximity to well-constrained offshore seismic basement depths (Brancolini et al., 1995) allows us to develop the method further. Most studies display their results as 2D profiles with the depth-scatter of solutions mentioned above, and simply use the tops of the clusters as the basement depth. By comparison with seismic basement, we have developed a reliable, automated method of 'draping' a surface over these depth-scattered solutions to produce a 3D surface. This process is described below.

Text S3. Tying magnetic basement to seismic basement

To validate the method described in Text S2 and address uncertainty we perform Werner deconvolution for OIB magnetics data (Figure 1b, Cochran et al., 2014) over the Ross Sea. Here, ice-free conditions have permitted shipborne seismic surveys to image basement depths in the region. These have been compiled by the Antarctic Offshore Acoustic Stratigraphy project (ANTOSTRAT) (Brancolini et al., 1995) (Figure 1b). The basement was not imaged for the deeper portions of the basins and data coverage of actual basement reflectors, versus interpolation between basement reflectors, is not reported. Werner deconvolution (Text S2) produces a series of many solutions (black dots in Figures 2 & S2) at each window along the line.

To achieve a basement surface, instead of a depth-scatter of solutions, solutions were filtered based on Werner window width (W) and the product of magnetic susceptibility and body width (parameter S). Filtered solutions (black circles, scaled to parameter S in Figures 2 & S2) were then horizontally binned with variable bin sizes (parameter B) (vertical grey lines in Figures 2 & S2). Bins with a minimum count of solutions (parameter C) were retained, and the depth of the bin center was set to the 95^{th}-percentile depth of the solutions in the bin. This removed spurious shallow solutions, while effectively retaining the 'top' of the magnetic signal. These bin centers (orange crosses in Figures 2 & S2) were then interpolated, producing our model of magnetic basement depths (orange line in Figures 2 & S2). The above filtering techniques removed the solutions above the basement, and the clustering technique fitted a surface over the remaining points, which represents the top of the basement. This interpolated line allowed a direct comparison between ANTOSTRAT seismic basement and OIB magnetic basement.

We varied each of the four parameters (W, S, B, and C) with 21 different values and conducted the above procedures for all unique combinations of them on OIB line 403, segments 1 and 3, in the Ross Sea (location in Figure 1b). This resulted in 194,481 iterations, for each of which we calculated a mean absolute difference at points every 5km between ANTOSTRAT seismic basement and the resulting OIB magnetic basement. We found the parameter values which produced the closest match between OIB magnetic basement and ANTOSTRAT seismic basement, as shown in Figures 2 & S2. These resulting values were a maximum Werner deconvolution window width (parameter W) of 10 km, a minimum product of magnetic susceptibility and body width (parameter S) of 1.0, a horizontal bin width (parameter B) of 36 km, and a minimum number of solutions per bin (parameter C) of 6. The median absolute misfit between OIB and ANTOSTRAT basement for the two line-segments was 480m (260m for Line 403.1 (Figure 2), and 1040m for Line 403.3 (Figure S2)). This equates to 11% of average ANTOSTRAT depths for the two lines. The close fit between the OIB magnetic basement and the ANTOSTRAT seismic basement both supports the validity of this method and gives us the parameters necessary to repeat this method for data over the RIS.

Text S4. Tying Ross Sea magnetic basement to Ross Ice Shelf magnetic basement

Having optimized our method to match OIB magnetic basement to ANTOSTRAT seismic basement in the Ross Sea (Text S3, Figures 2 & S2), we now optimize the method to match ROSETTA-Ice magnetic basement to OIB magnetic basement. This additional optimization is necessary due to differences in processing and survey design, including flight elevations, speed, aircraft, mounting equipment used, and frequency of recording. With the optimized parameters for OIB data (Text S3), we calculate magnetic basement for OIB flight 404 over the ice shelf. We treat this as the 'true' basement and update the filtering and clustering parameters (Text S2) to minimize the misfit between OIB basement and the resulting ROSETTA-Ice basement. This tuning was performed on ROSETTA-Ice lines 590 and 650, which were coincident with segments from OIB line 404 (location in Figures 1b & S4). Optimal parameters to match ROSETTA-Ice solutions to OIB basement are found to be W<26 km, S>1.2, B=36 km, and C>40, resulting in a median absolute misfit between OIB basement and ROSETTA-Ice solutions of 400 m (630m for line 404.590 (Figure S3e) and 310m for line 404.590 (Figure S3f). This equates to 18% of OIB depths for the two lines. With these parameters which best match ROSETTA magnetic basement to OIB magnetic basement, we performed the same procedure on all the ROSETTA-ice flight lines. A selection of these lines, and the two ties to OIB 404, are shown in Figure S3. All ROSETTA-ice flight line solutions are available as images at the PANGAEA link.

Text S5. Gridding, merging, and filtering

The above processes were performed on all ROSETTA-ice flight lines (white lines in Figure S4), including the N-S tie lines at ~55 km spacing. Where the tie lines crossed over the E-W flight lines, some resulting basement solutions (black dots in Figure S4) are nearby those from the crossing line. Since we are interested in the shallowest magnetic signals, we have retained only the shallowest solution with 8km cells across our region. Since bin widths (parameter B) were set to 36 km, the nearest solutions along individual lines were further apart than the 8km cell. The closest spacing of E-W flight lines was 10

km, so this process only affected solutions at the crossover between N-S and E-W lines. These points were then gridded with a 5 km cell size and a minimum curvature spline with a tension factor of 0.35 (Smith & Wessel, 1990) (Figure S4). This grid was then merged with a Ross Sea seismic basement grid. The Ross Sea grid, while mostly ANTOSTRAT data, was sourced from a regional compilation of sediment thicknesses (Lindeque et al., 2016, Wilson and Luyendyk 2009) we have subtracted from bathymetry depths (Morlighem et al. 2020) to achieve basement depths. Where the grids overlap near the ice shelf edge, we retain our RIS values. To aid in the merging at the overlaps, and to match RIS basement wavelengths to the characteristic basement wavelengths of ANTOSTRAT, we filtered the merged grid with an 80 km Gaussian filter (Figure 3a). This filtering was performed with a variety of wavelengths (20-120 km), where we found filters < 80 km didn't significantly alter the regional basement, while filters > 80 km excessively smoothed the basement topography. A few locations with anomalously shallow basement were set equal to BedMachine bathymetry.

Text S6. Sediment thickness and β-factor calculations

With the regional basement model (Figure 3a) including RIS magnetic basement and offshore seismic basement, we calculated sediment thickness (Figure 3b) by subtracting the grid from Bedmachine bathymetry depths (Figure1a & S1e, Morlighem et al. 2020). Previous estimates of sediment thickness for the sub-RIS come from the extrapolation of gravity anomalies with bathymetry trends (Wilson and Luyendyk, 2009). These were included in the Lindeque et al. (2016) compilation (Figure S1d). Eocene-Oligocene boundary paleotopographic reconstructions (Wilson et al., 2012, Paxman et al., 2019) assumed this sediment estimate was post-Eocene and used it as their maximum sub-RIS sediment thickness, incorporated into their minimum surface reconstruction. The thickness of sediment affects onshore erosion estimates, surface raising due to deposition, and isostatic surface subsidence to due loading. For their maximum paleotopographic reconstructions, they used a thinner sediment model, with the same general trends (Wilson & Luyendyk, 2009). Figure S1 (c, d, & f) shows the comparison between the sediment thickness models. Figure S1f colorbar histogram shows the distribution, with our values having a mean thickness ~115m greater than the past model. Yet, along the Siple Coast, we show much greater discrepancies, up to 2 km thicker.

β-factor, the ratio of initial crustal thickness to final crustal thickness, is useful for quantifying the thinning of crust in extensional settings. We calculate a distribution of β-factors beneath the RIS by assuming a uniform initial crustal thickness and dividing it by current crustal thickness. We pick an initial crustal thickness of 38 km, which represents a global average for un-thinned plateau-type crust (Mooney et al., 1998), and has been used for the West Antarctic Rift System β-factor calculations (Müller et al., 2007). For the final (current) crustal thickness, we use a continent-wide Moho model from surface wave observations to define the bottom of the crust (An et al., 2015). For the top of the crust, we use our resulting RIS basement grid.

Text S7. Uncertainties

We estimated a representative uncertainty for our basement model by examining the misfit of our modeled basement compared to offshore seismic basement depths

(Brancolini et al., 1995). We did this by sampling our OIB magnetic basement estimate and the coincident ANTOSTRAT basement at 1 km intervals along lines 403.1 and 403.3 (Figures 2 and S2) and compared the values. The resulting absolute values of the differences don't exhibit a normal distribution (Figure S6a); therefore, we use the median of the absolute misfit (+/-480m) as the basement model uncertainty. This equates to 22% of average basement depths for the sub-RIS. We performed a similar analysis between OIB magnetic basement and ROSETTA-Ice magnetic basement for coincident lines 590 and 650 (Figure S3 e & f). This resulted in a median absolute misfit of 400m (Figure S6b). Tinto et al. (2019) report an uncertainty of 68m for their bathymetry model. Incorporating this with our basement model gives an uncertainty of 550m (37% of average thickness) for our sediment thickness results. Comparison with sub-RIS sediment thickness and distribution results from a variety of methods, including active source seismic surveys (Table S1 and references within), seismic radial anisotropy (Zhou et al., 2022), geophysical machine learning (Li et al. 2021), and magnetotelluric surveying (Gustafson et al. 2022), all show general agreement with our results.

Name	Reference	Seismic sediment thickness (m)	Magnetic sediment thickness (m)	Absolute difference (m)
CIR	Rooney et al. (1987)	400	514	114
I10S	Robertson and Bentley (1989)	750+/-100	1281	818
J9DC	Greischar et al. (1992)	1350	770	580
BC	Robertson and Bentley (1989)	1900+/-400	1082	818
RI	Greischar et al. (1992)	850	822	28
C49	Crary (1961)	754	1162	408
LAS	Crary (1961)	1325	1799	474
Q13	Greischar et al. (1992)	255+/-145	721	466

Table S1. Previous seismic sediment thickness results for the Ross Ice Shelf. Stations names are labeled in Figure 3b. Magnetic sediment thickness column shows our sampled results at the location of each station. Comparing the seismic estimates with our sediment thickness at the eight stations gives a median absolute misfit of 470m.

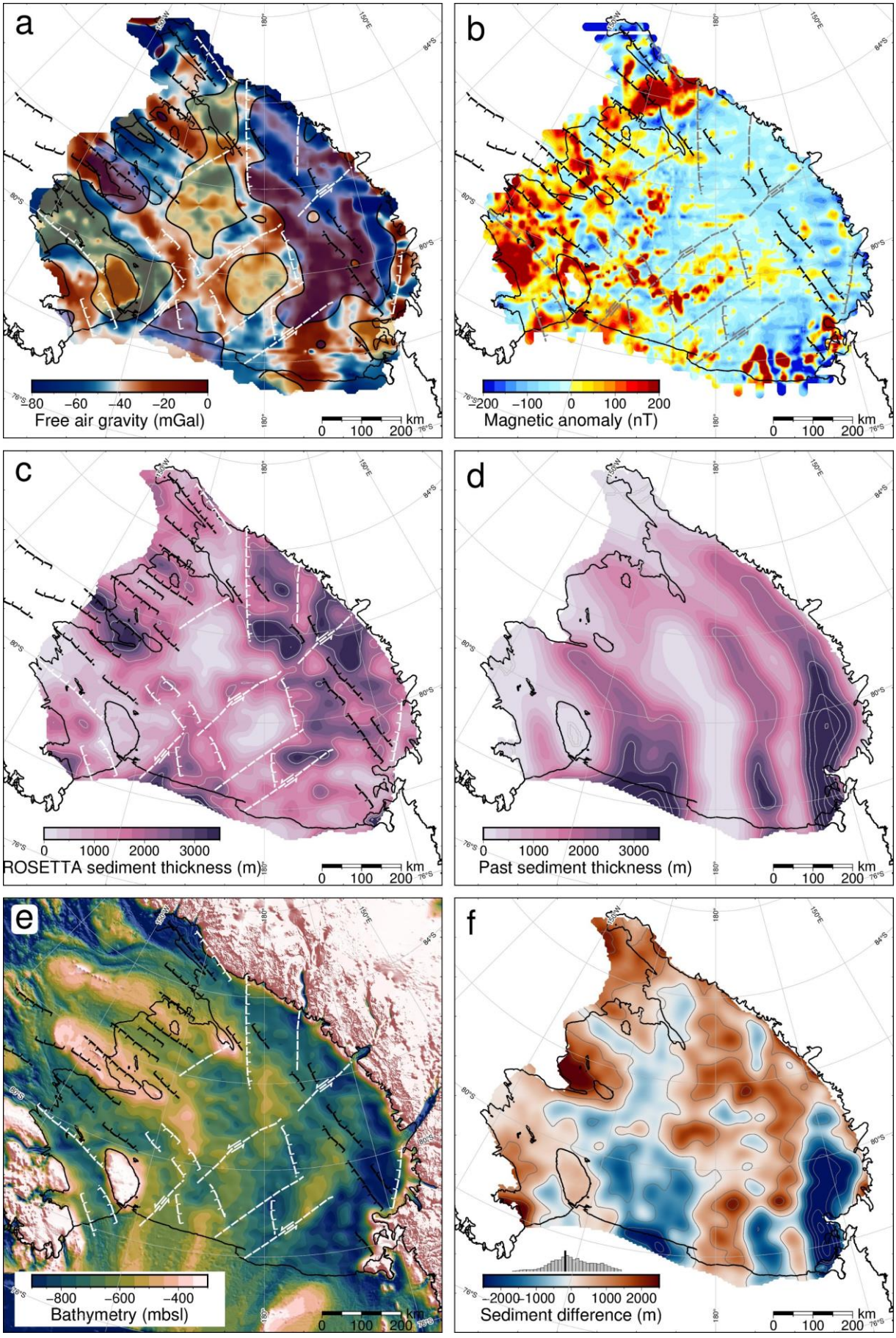
a
−80 −60 −40 −20 0
Free air gravity (mGal)
b
−200 −100 0 100 200
Magnetic anomaly (nT)
c
0 1000 2000 3000
ROSETTA sediment thickness (m)
d
0 1000 2000 3000
Past sediment thickness (m)
e
−800 −600 −400
Bathymetry (mbsl)
f
−2000 −1000 0 1000 2000
Sediment difference (m)
0 100 200 km

Figure S1. (a) ROSETTA-Ice free air gravity (Tinto et al., 2019). Shaded yellow regions are shallow basement (<~1600 mbsl), shaded blue regions are deep basement (>~2600 mbsl). **(b)** ROSETTA-Ice airborne magnetic anomaly data (Tinto et al., 2019). **(c)** Sediment thickness from this study (same as Figure 3b), with 1 km contours. **(d)** Sediment thickness from a regional compilation (Text S6, Lindeque et al., 2016, Wilson & Luyendyk, 2009), with 1 km contours. **(e)** Bedmachine2 bathymetry (Morlighem et al., 2020), from which sediment thickness in (c) was calculated. **(f)** Difference between (c) and (d). Red signifies our results have more sediment, while blue signifies our results have less sediment. Histogram shows data distribution, with mean value (black) at 115m. Inferred faults in a),b),c), and e) same as Figure 4a. Grounding line and coastlines in black (Rignot et al., 2013). Projection is Antarctic Polar Stereographic: EPSG 3031.

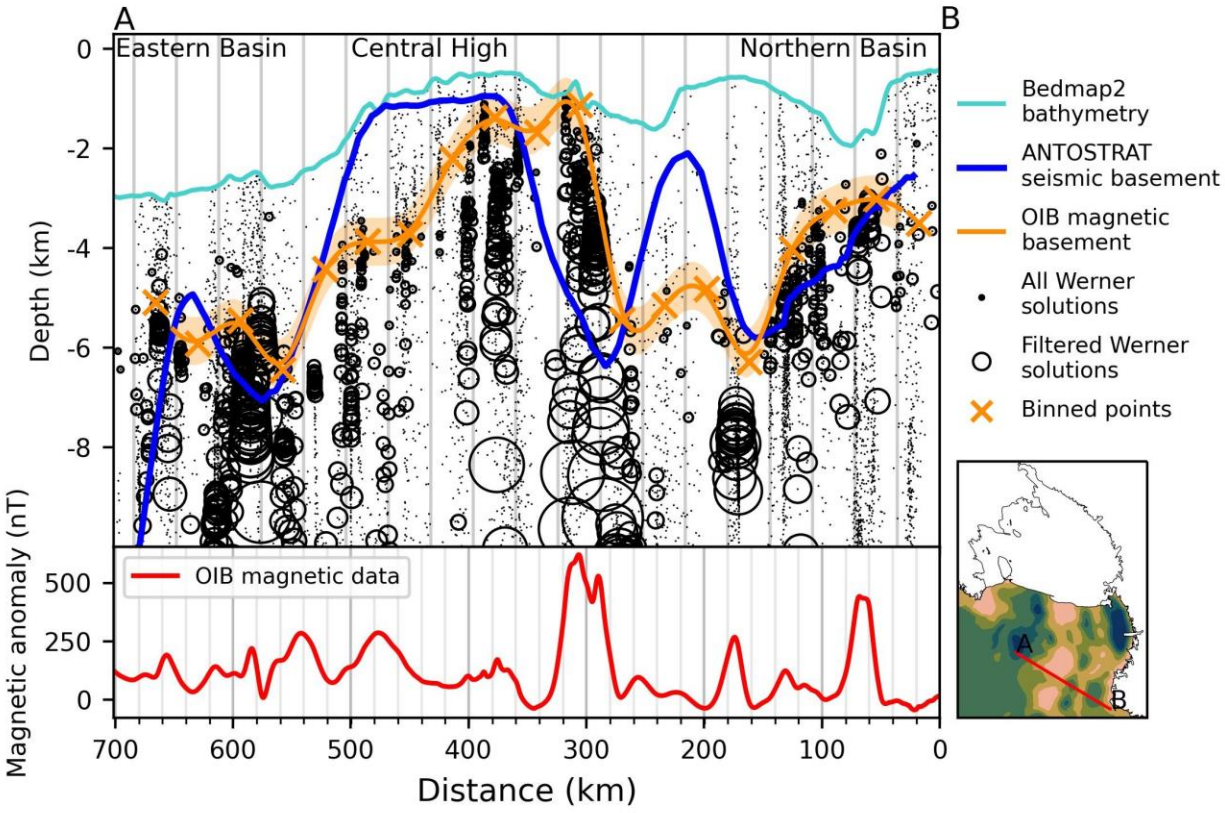

Figure S2. Ross Sea magnetic and seismic basement comparison. Operation IceBridge airborne magnetic data (lower panel) from segment 403.3 (Figure 1b). Small dots show Werner deconvolution solutions, which were filtered based on parameters S and W (Text S2) to produce black circles, which are scaled to parameter S. These circles were binned at a width equal to parameter B, shown by the vertical grey lines in the upper panel. Orange crosses show bin centers, which were fitted to a line to facilitate the comparison between the magnetic basement (orange line) and seismic basement (blue line). Orange band shows +/- 480m uncertainty for the basement model. Ross Sea basement features are labeled on top.

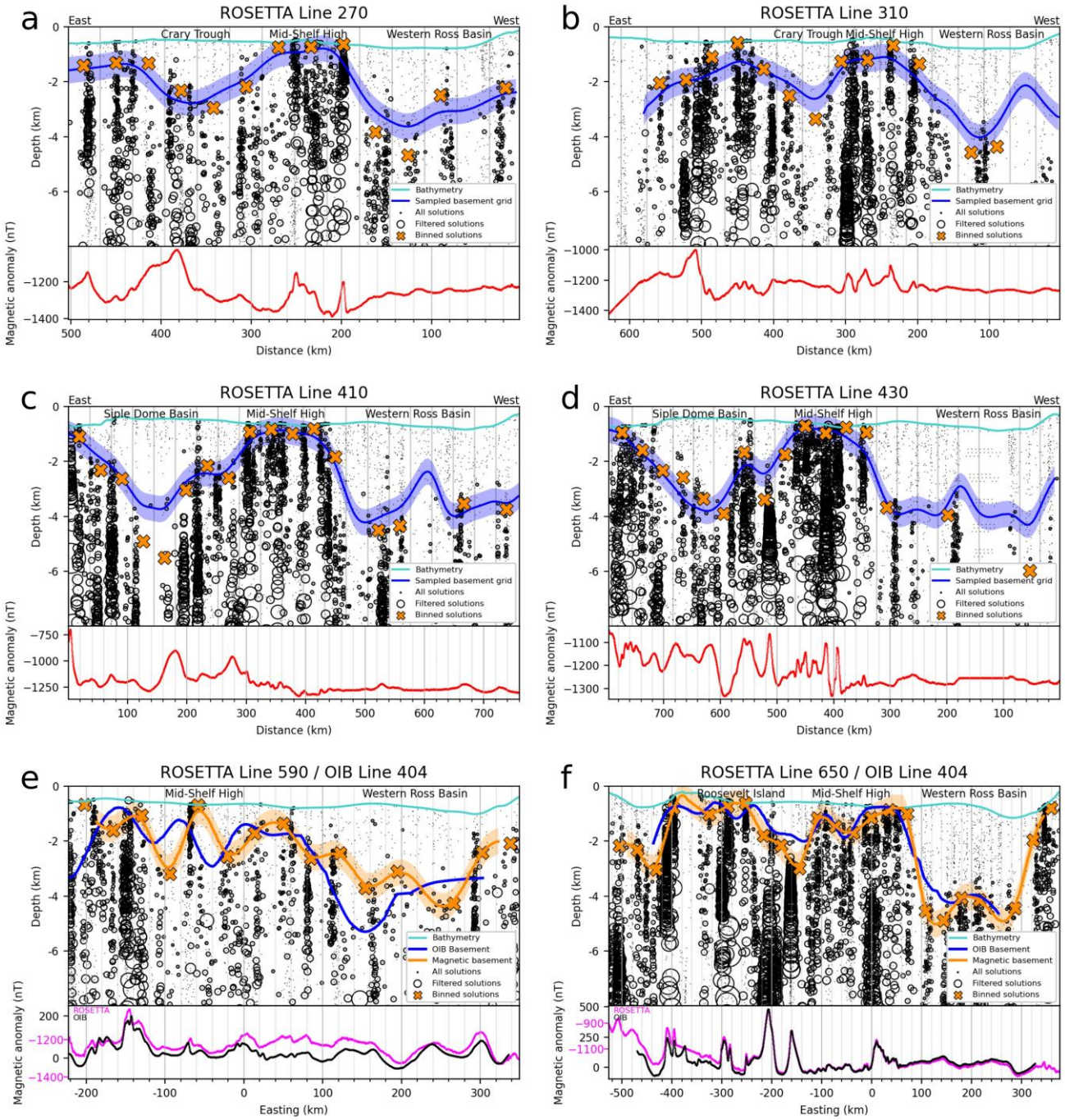

252 **Figure S3.** Werner deconvolution solutions for a selection of ROSETTA-Ice lines,
253 locations highlighted in Figure S4. Bathymetry from Bedmap2 (Fretwell et al., 2013). Dots,
254 circles, and vertical grey lines same as Figure S2. **a-d)** Comparison between magnetic
255 basement before and after filtering and gridding. Orange crosses are magnetic basement
256 solutions, shown as black dots in Figure S4, and highlighted for these lines. Orange line
257 with uncertainty bounds is fitted to these solutions. Blue lines are magnetic basement
258 sampled from the grid of Figure 1a, after gridding and filtering. Red lines show
259 ROSETTA-Ice magnetics data. **e-f)** Comparison between magnetic basement resulting
260 from Werner deconvolution of coincident OIB and ROSETTA-Ice flight lines. Location is
261 shown in Figures 1b and S4. These two lines were used to tie the ROSETTA-Ice survey to

the OIB survey (Text S4). Blue lines are OIB magnetic basement results, orange crosses and fitted orange lines with uncertainty bands are ROSETTA-Ice magnetic basement. ROSETTA-Ice (pink) and OIB (black) magnetics data are shown in lower panels.

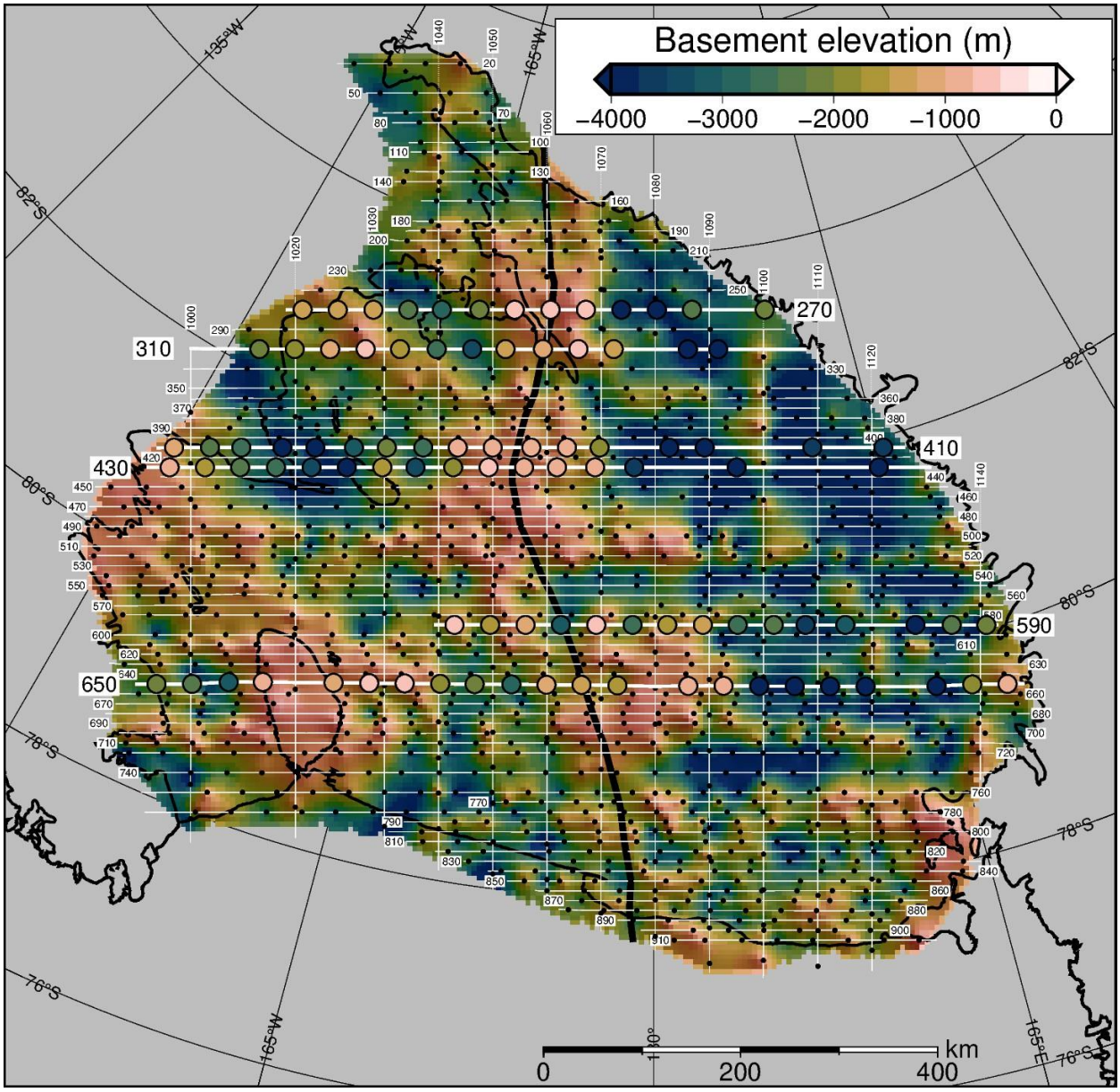

Figure S4. Unfiltered magnetic basement. Point solutions (black dots here, orange crosses in Figure S3) along ROSETTA-Ice flight lines (labeled) were gridded with a 5km cell size and a minimum curvature spline with a tension factor of 0.35. Figure S3 flight lines (bold white) and point solutions (colored circles) are shown. Black line through the Mid-Shelf High shows the East-West Antarctic divide used in colorbar histograms of Figures 3 and 4a. Grounding line and coastlines in black (Rignot et al., 2013).

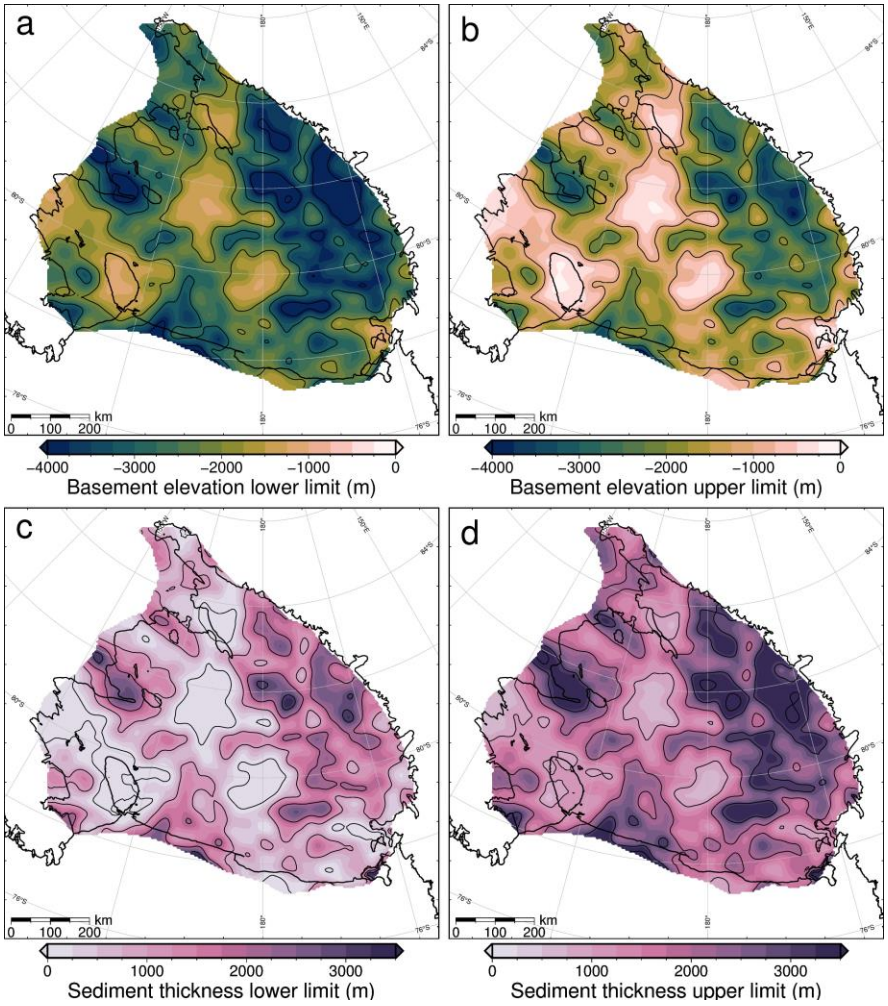

271 **Figure S5.** Upper and lower limits of uncertainty applied to **a-b)** magnetic basement and
272 **c-d)** sediment thickness. See Text S7 for how these uncertainties were determined.

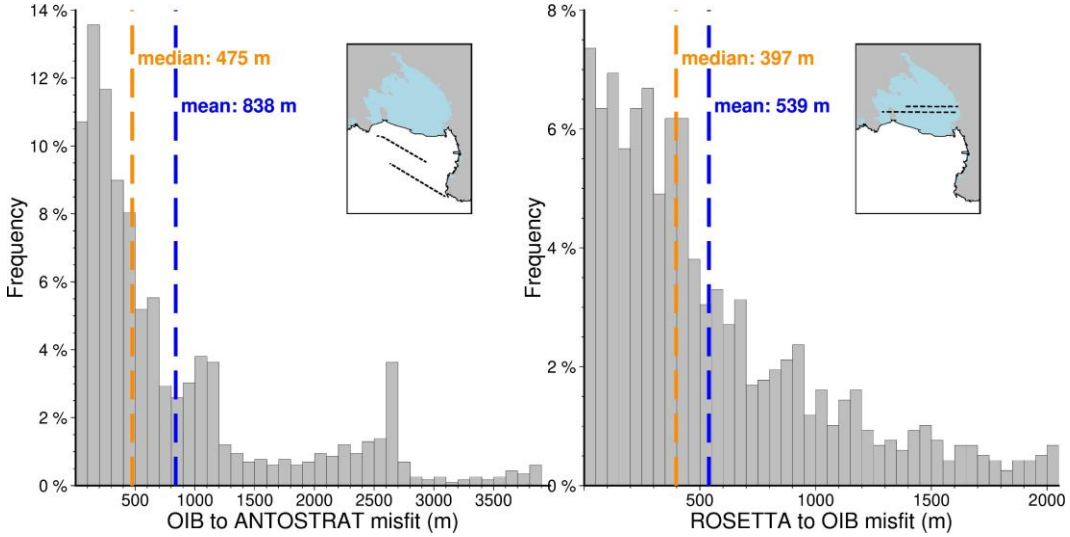

273 **Figure S6.** Misfit distributions for comparisons between **a)** OIB magnetic basement and
274 ANTOSTRAT seismic basement and between **b)** ROSETTA magnetic basement and OIB
275 magnetic basement. Inset maps show the locations of flight lines. Basement models were
276 sampled at 1km intervals for the comparison.